inorganics

MDPI

Article

Synthesis, Photophysical Properties, and Toxicity of *o*-Xylene-Bridged Porphyrin Dimers

Kseniya A. Zhdanova [1,*], Andrey A. Zaytsev [1], Margarita A. Gradova [2], Oleg V. Gradov [2], Anton V. Lobanov [2], Alexander S. Novikov [3,4,*] and Natal'ya A. Bragina [1]

[1] Institute of Fine Chemical Technology, MIREA—Russian Technological University, Vernadsky Pr., 86, 119571 Moscow, Russia; chemist.andrew@mail.ru (A.A.Z.); n.bragina@mail.ru (N.A.B.)
[2] N.N. Semenov Federal Research Center for Chemical Physics, Russian Academy of Sciences, Kosygin St., 4, 119991 Moscow, Russia; m.a.gradova@gmail.com (M.A.G.); o.v.gradov@gmail.com (O.V.G.); avlobanov@mail.ru (A.V.L.)
[3] Institute of Chemistry, Saint Petersburg State University, Universitetskaya nab. 7–9, 199034 Saint Petersburg, Russia
[4] Research Institute of Chemistry, Peoples' Friendship University of Russia (RUDN University), Miklukho-Maklaya St., 6, 117198 Moscow, Russia
* Correspondence: zhdanova_k@mirea.ru (K.A.Z.); a.s.novikov@spbu.ru or novikov-as@rudn.ru (A.S.N.); Tel.: +7-9261126692 (K.A.Z.); +7-9819580247 (A.S.N.)

Abstract: In this work, a number of new porphyrin dimers coupled with spacers based on α,α′-dibromo-*o*-xylene were synthesized and characterized by ^{1}H, ^{13}C NMR, ^{1}H-^{1}H COSY NMR, UV-vis-spectroscopy, and MALDI-TOF mass spectrometry. The initial A3B-type hydroxy-substituted porphyrins form dimer structures with high yields of 80–85%, while the use of amino-substituted porphyrins as starting compounds leads to the heterocyclization and formation of N-heterocycle fused porphyrins. For porphyrin dimers, photophysical properties and quantum yields of singlet oxygen were investigated. The peripheral alkoxy-substituents increase fluorescence quantum yield in comparison with the unsubstituted compounds. Also, it was found that dimers are characterized by lower singlet oxygen quantum yields compared to the corresponding monomers. Model aggregation experiments in micellar systems demonstrate stabilization of the photoactive monomolecular form of all the porphyrins, using nonionic surfactant Triton X-100. Cytotoxicity of received dimers shows high inhibition against HEK293T cells in the absence of light.

Keywords: *meso*-arylporphyrins; porphyrin dimers; synthesis; singlet oxygen; aggregation; solubilization; dark toxicity

check for updates

Citation: Zhdanova, K.A.; Zaytsev, A.A.; Gradova, M.A.; Gradov, O.V.; Lobanov, A.V.; Novikov, A.S.; Bragina, N.A. Synthesis, Photophysical Properties, and Toxicity of *o*-Xylene-Bridged Porphyrin Dimers. *Inorganics* **2023**, *11*, 415. https://doi.org/10.3390/inorganics11100415

Academic Editors: Wolfgang Linert, Gabriel García Sánchez, David Turner and Koichiro Takao

Received: 5 September 2023
Revised: 25 September 2023
Accepted: 10 October 2023
Published: 19 October 2023

Copyright: © 2023 by the authors. Licensee MDPI, Basel, Switzerland. This article is an open access article distributed under the terms and conditions of the Creative Commons Attribution (CC BY) license (https://creativecommons.org/licenses/by/4.0/).

1. Introduction

Porphyrins are one of the key compounds in nature due to their role in hemoglobin, myoglobin, chlorophyll, and cytochromes [1–3]. Due to their chemical structure, unique optical and electrochemical properties, high thermal stability, and advanced chemistry, porphyrins have gained a broad application in various fields of medicine and techniques [4–6]. Moreover, depending on porphyrins' molecular structure, there is the possibility of modulating their photophysical properties. Thus, peripheral substituents can alter porphyrins' structural and electronic properties [7–11]. In this regard, synthesis of multi-porphyrin systems has been actively studied by many researchers, owing to their great potential. Specific macrocycle's ordering in space of multi-porphyrins enables improvement of their physico-chemical characteristics and expansion of the range of their applications [12]. There are two main approaches to obtain multi-porphyrin assemblies: the use of noncovalent or covalent binding via different bridges [13].

Noncovalent binding is based on a supramolecular methodology driven by the self-assembly of molecules [14]. In this case, multi-porphyrin arrays can be built using a

set of non-covalent interactions such as coordination [15,16], electrostatic or hydrogen interactions [17]. Self-assembly of metalloporphyrins via coordination interactions with nitrogenous ligands is one of the widespread approaches to receiving multi-porphyrin complexes. Thus, such supramolecular coordination multi-porphyrin arrays were received using pyridyl-containing multidentate ligands [15,18]. This approach is distinguished by the simplicity of synthesis and the possibility to control the spatial orientation of chromophores by means of the linker type. However, there are disadvantages in the stability of the complex assembly [12].

Covalent binding relies on the creation of a strong connection between macrocycles by means of a certain geometry bridge [19]. Covalent binding has advantages in the reliability of the obtained complexes and the possibility to extend π-conjugation [20], but such an approach often involves complicated synthetic procedures, isolating steps of final compounds and low final yields. At present, such covalently bound dimers for the purposes of photovoltaics [21–25], medicine [26–28], and catalysis [29,30] are of increasing interest. The properties of such systems primarily depend on the porphyrin structure and the type of linker that binds the porphyrins together. Among covalently linked dimers, porphyrins linked via bridges of various types have been obtained: π-conjugated bridge [27], triazole fragment [31], *meso-meso*-bridged porphyrins [22,23,32], β-β-substituted dimers [33], and cofacial porphyrin dimers [34,35]. Therefore, elaboration of effective and simple synthetic routes towards the covalent binding of porphyrins is of particular interest.

Previously, authors [36,37] demonstrated the influence of the nature of the *o*-xylene spacer, metal-complexing ions, and peripheral substituents on the spectral properties exhibited by these covalently coupled macrocyclic compounds using bi- and poly-nuclear clamshell-type phthalocyanines. This work is devoted to the development of methods for the synthesis of *o*-xylene-bridged porphyrin dimers and their Zn(II) complexes, as well as the study of their physicochemical and aggregation properties and dark cytotoxicity on HEK293 cells. The structure of the target compounds differs from the long-chain alkoxyl substituents and the central metal atoms.

2. Results and Discussion

2.1. Synthesis of the Initial A3B Porphyrins and Their Dimers

Previously, we have demonstrated the efficiency of the monopyrrole condensation method using prefunctionalized alkoxy-substituted benzaldehydes in order to obtain A3B-type porphyrins with the final yields of 10–13% [38–40]. Porphyrins with amino- and hydroxy-groups 1–3 were synthesized according to a modified Adler method in a mixture of acetic acid, propionic acid, and nitrobenzene. Their Zn (II) complexes 1,2-Zn were synthesized by the standard procedure, using excess zinc acetate dihydrate in a methanol/DCM mixture.

The introduction of alkoxy substituents at the stages of benzaldehyde's synthesis enables simplification of the synthetic scheme, and the difference in polarity between hydroxyl- or amino-substituents facilitates isolation of the target products; thus, high yields of the target asymmetrical porphyrins are achieved. Figure 1 shows the structures of the starting porphyrins bearing NH_2- and OH-reactive groups.

Further in this work, *o*-xylene linked dimers were obtained. The target dimers were prepared by nucleophilic substitution of the bromine atoms in α,α′-dibromo-*o*-xylene with zinc porphyrinate residues containing a free hydroxyl group (Scheme 1). The reaction of Zn(II) complexes and free-base porphyrins was performed in the presence of excess base (5 eq.). The reaction was carried out in DMF for 5 h at 100 °C. Several inorganic and organic bases were used: K_2CO_3, Cs_2CO_3, and DIPEA (Scheme 1, Table 1). The highest yield was achieved with cesium carbonate (85%); for potassium carbonate, it was 40%, and in the case of DIPEA, a trace product was obtained. Along with the disubstituted product, the formation of up to 10% of a minor monosubstituted porphyrin was observed.

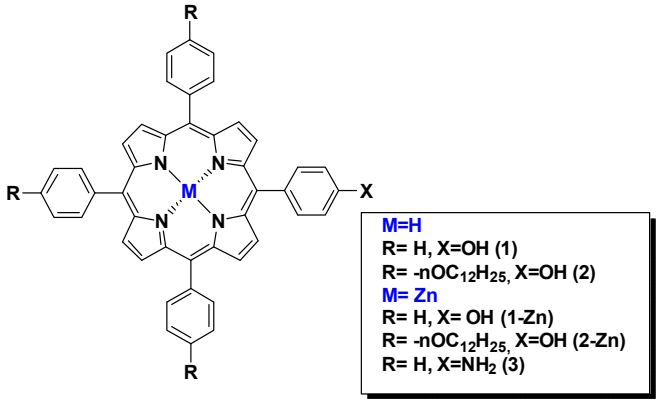

Figure 1. Initial A3B porphyrins for the synthesis of dimers.

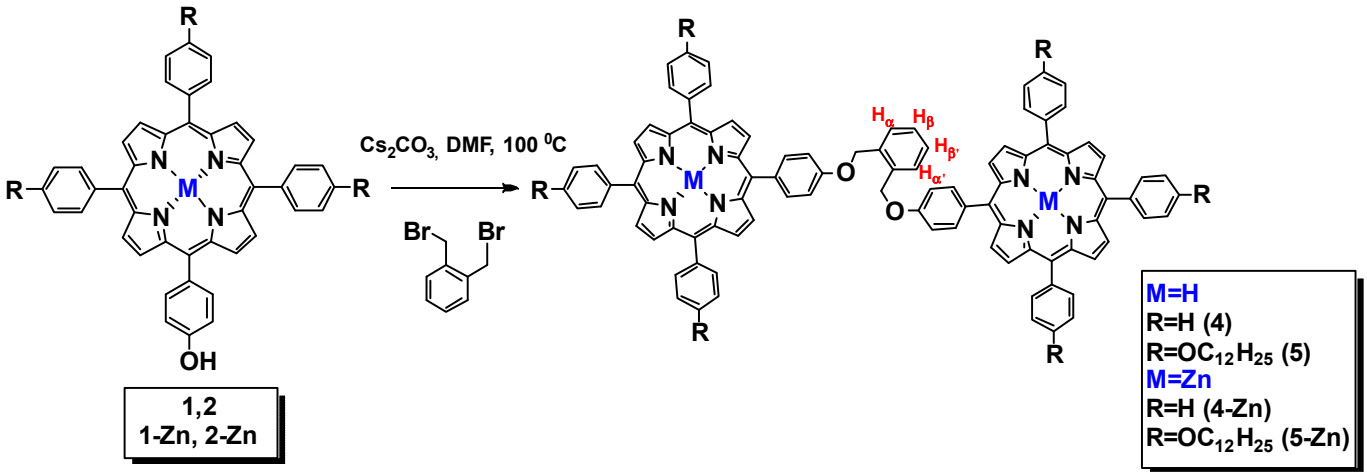

Scheme 1. Synthesis of porphyrin-based dimers 4, 5, 4-Zn, 5-Zn.

Table 1. Reaction conditions and yields of 4, 5, 4-Zn, 5-Zn in DMF.

Compound	Base	Reaction Temperature °C	Reaction Time, h	Yield, %
4	K_2CO_3	100	5	35
	Cs_2CO_3	100	5	82
	DIPEA	100	5	traces
5	K_2CO_3	100	5	32
	Cs_2CO_3	100	5	85
	DIPEA	100	5	traces
4-Zn	K_2CO_3	100	5	40
	Cs_2CO_3	100	5	85
	DIPEA	100	5	traces
5-Zn	K_2CO_3	100	5	45
	Cs_2CO_3	100	5	89
	DIPEA	100	5	traces

The structures and individuality of the obtained dimers and their metal complexes were confirmed by TLC, UV-vis, ^{1}H, ^{13}C NMR spectroscopy, and mass spectrometry (Figures S1–S13, Supplementary Material). The ^{1}H-^{1}H COSY experiments were used to correlate the protons of the *o*-xylene group. The position of the signals corresponding to the H_α- and H_β-protons of the xylene fragment at 7.34–7.36 ppm and 7.17–7.19 ppm (two doublets), respectively, were determined. The signals of the β-pyrrole protons in the ^{1}H NMR spectra of dimers are observed at 8.70–9.10 ppm, four methylene protons of benzyl fragment are in the 5.5–6.0 ppm region (singlet), and the aliphatic proton's signals

of compounds 5 and 5-Zn are in the strong field region of 2.30–3.30 ppm (multiplets). In the ^{1}H NMR spectra of Zn complexes, the disappearance of the NH protons in the negative part of the spectrum was observed.

In contrast to the hydroxyporphyrins, the interaction of amino porphyrin 3 with similar binding reagents leads to the heterocyclization of *o*-xylene fragment (Scheme 2). Thus, treatment of compound 3 (2 eqv) with one equivalent of α,α′-dibromo-*ortho*-xylene in the presence of various inorganic bases did not result in the dimer formation. Instead, a competitive heterocyclization reaction proceeded with the formation of compound 6 in 80% yield. The structure of compound 6 was confirmed by the ^{1}H NMR spectrum as well as MALDI-TOF mass spectrometry data. In the ^{1}H NMR spectrum, the presence of a singlet signal of four pyrrolidine protons at 4.98 ppm was observed (Figures 2, S14 and S15 Supplementary Material). This reaction behavior can be explained by the higher nucleophilicity of the nitrogen atom of the amino group compared to the hydroxyl group, leading to heterocyclization of the initial amino porphyrin. The proposed mechanism of this reaction is shown in Scheme 3.

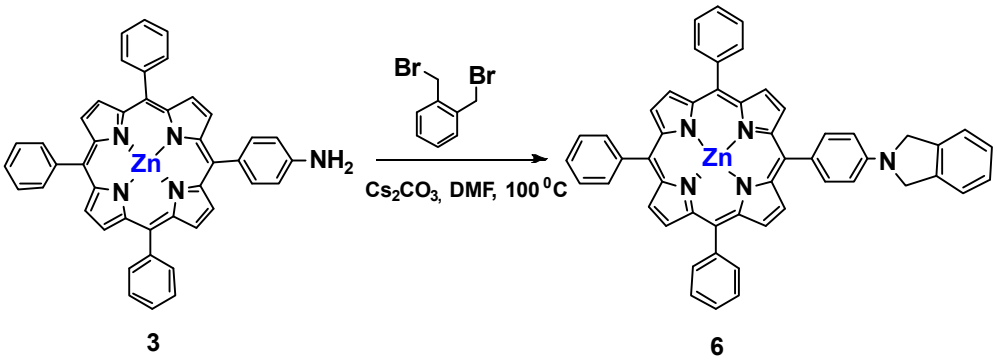

Scheme 2. Synthesis of N-heterocycle fused porphyrins based on the initial porphyrin 3.

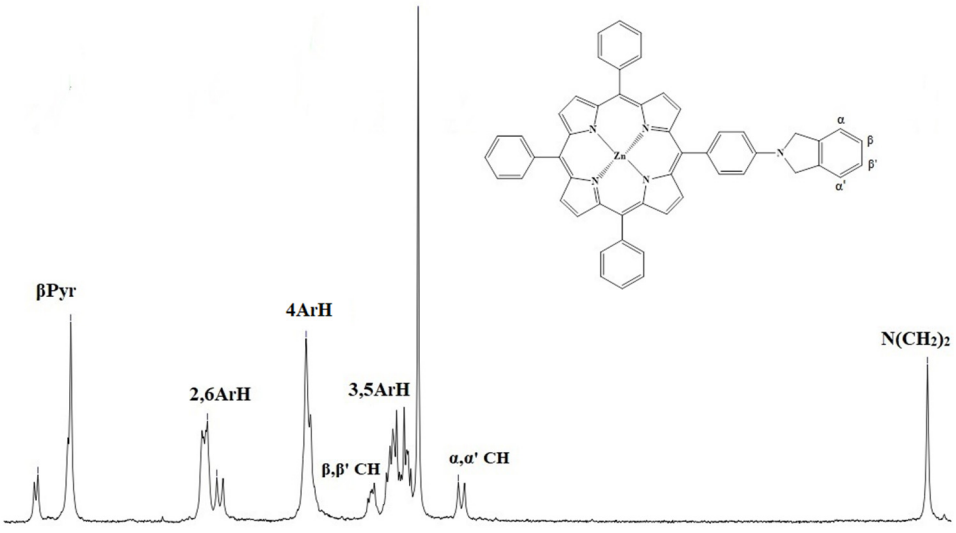

Figure 2. Fragment of ^{1}H NMR spectrum of porphyrin 6.

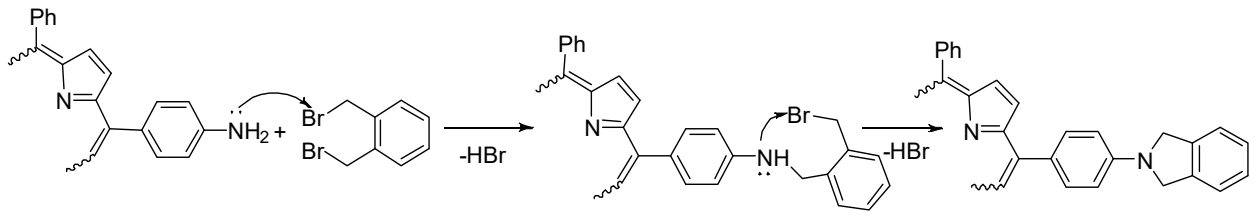

Scheme 3. The proposed mechanism of heterocyclization.

2.2. Photophysical Properties

All the obtained compounds were characterized by UV-visible spectroscopy and fluorimetry. The data presented in Table 2 show that in DMF, the shape and position of the absorption and emission bands are almost identical for monomers and their corresponding dimers. However, fluorescence quantum yields of the dimers appear to be higher than for the monomers in the case of zinc complexes or comparable to them in the case of the metal-free derivatives. The nature of the peripheral substituents in the macrocycle also contributes to the fluorescence quantum yield values: Φ_F = 0.06 is observed for the initial *meso*-phenylporphyrins 1 and corresponding dimer 4, while Φ_F = 0.12 is observed for their alkoxy-substituted derivatives 2 and corresponding dimer 5 (Table 2).

Table 2. Photophysical properties of received compounds in DMF *.

	1	**4**	**1-Zn**	**4-Zn**	**2**	**5**	**2-Zn**	**5-Zn**
λ_{max}, nm	416	418	428	426	422	422	426	426
$\Delta\lambda_{1/2}$, nm	12	16	11	13	14	12	10	13
$\lambda_{em1,2,}$ nm	651, 718	652, 717	606, 659	609, 662	661, 724	661, 724	614, 665	610, 662
I_1/I_2	3.11	3.15	1.46	1.64	4.26	3.81	2.36	1.58
Φ_F [a]	0.061	0.062	0.011	0.020	0.118	0.115	0.028	0.044
Φ_Δ [b]	0.64	0.49	0.76	0.68	0.50	0.46	0.81	0.71

* The error of the quantum yield determination is 10%. [a] Φ_F: quantum fluorescence yield is determined using TPP in toluene (Φ_F = 0.11) as a standard. [b] Φ_Δ: quantum yield of singlet oxygen in DMSO.

All the dimers are characterized by lower singlet oxygen quantum yields compared to the corresponding monomers. This difference can be attributed to the spatial colocalization of the linked porphyrin macrocycles, resulting in the increased probability of the non-radiative decay and self-quenching of the excited states, resulting in the decreased triplet state and singlet oxygen quantum yields. Overall, zinc complexes are characterized by higher singlet oxygen quantum yields and lower fluorescence intensity compared to the metal-free porphyrins, which agrees well with the available literature data [41].

2.3. Aggregation Behavior

In contrast to the organic solvent medium, all the compounds studied in water exhibit an increased tendency to aggregation, which is accompanied by a decrease in the intensity and significant broadening of the Soret band, as well as by the luminescence quenching and a significant decrease in the efficiency of singlet oxygen generation. For overcoming this problem, spectral-luminescent properties in model micellar systems of different charge were compared for the target compounds during solubilization studies (Figure 3, Table 3, Figures S16–S20 Supplementary Material).

Among the model surfactants tested, only nonionic surfactant Triton X-100 provides effective stabilization of the photoactive monomolecular form of all the porphyrins in micellar systems (Figure 3). Such results are in agreement with our previously obtained data [42]. In the micelles of ionic surfactants (SDS, CTAB), only partial solubilization is observed for the porphyrin monomers, while both anionic SDS and cationic CTAB failed to provide effective solubilization of the dimers in aqueous media. This may be due to the neutral nature of the porphyrin molecules, which prevents them from ionic binding to the micellar surface, as well as to the large size of the porphyrin dimers compared to the hydrodynamic diameter of a single ionic surfactant micelle. At the same time, in contrast to DMF, the emission band at 660 nm is predominant in the fluorescence spectra of all zinc dimers in micellar media (Table 3, Figures S16–S20 Supplementary Material).

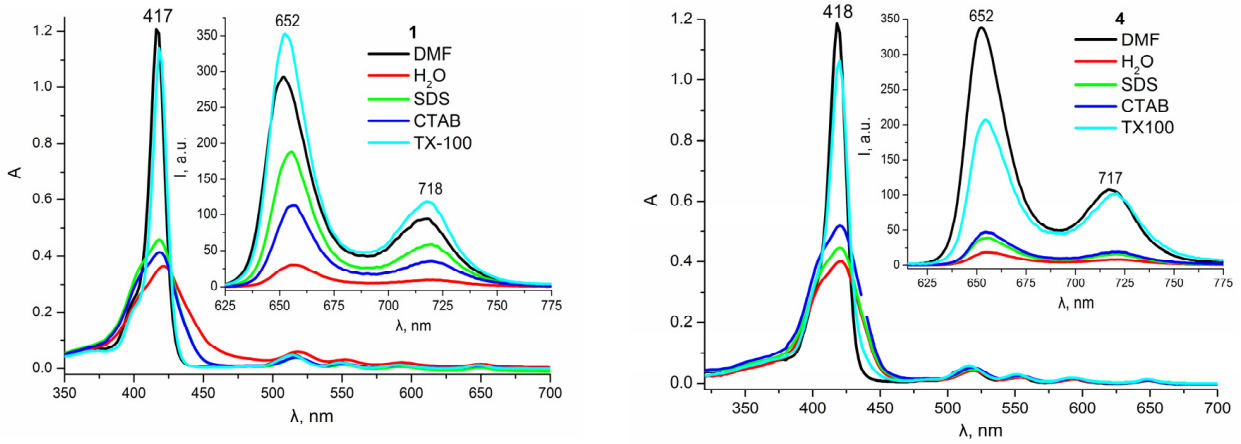

(**A**) (**B**)

Figure 3. Electronic absorption spectra and the corresponding fluorescence spectra (insert) for porphyrin 1 (**A**) and dimer 4 (**B**) in DMF, water, and micellar surfactant solutions.

Table 3. Spectral properties of received compounds in water and in micellar systems.

	1	**4**	**1-Zn**	**4-Zn**	**2**	**5**	**2-Zn**	**5-Zn**
				H_2O				
λ_{max}, nm	422	420	428	428	422	424	430	428
$\Delta\lambda_{1/2}$, nm	46	44	36	32	37	33	37	33
$\lambda_{em1,2}$, nm	655, 717	655, 721	610, 652	607, 655	658, 724	661, 725	613, 644	611, 647
I_1/I_2	3.00	2.38	0.52	0.65	2.12	3.35	0.98	0.53
				SDS				
λ_{max}, nm	418	420	424	426	424	424	429	426
$\Delta\lambda_{1/2}$, nm	38	41	31	31	31	35	38	32
$\lambda_{em1,2}$, nm	655, 719	656, 721	606, 656	608, 653	659, 733	660, 723	611, 644	608, 648
I_1/I_2	3.19	2.50	1.06	0.55	1.07	3.05	0.76	0.61
				CTAB				
λ_{max}, nm	418	420	424	426	424	424	432	426
$\Delta\lambda_{1/2}$, nm	39	40	29	32	35	36	42	34
$\lambda_{em1,2}$, nm	657, 719	655, 719	610, 650	608, 650	663, 724	660, 724	616, 650	610, 652
I_1/I_2	3.14	2.47	0.40	0.28	2.93	2.92	0.57	0.31
				TX-100				
λ_{max}, nm	418	420	426	426	424	422	428	426
$\Delta\lambda_{1/2}$, nm	13	17	11	16	22	20	15	16
$\lambda_{em1,2}$, nm	652, 718	654, 719	605, 657	610, 650	660, 724	659, 723	613, 663	609, 653
I_1/I_2	2.98	2.08	1.27	0.33	3.89	3.46	1.96	0.57

2.4. Surface Morphology of the Particles

The obtained powders of target compounds visually appeared different in shape and structure of particles. Obviously, the presence of long-chain alkoxy substituents affect the morphology of crystallization products. SEM images of the individual particles were obtained for powders of the synthesized monomers 1-2 and dimers 4,5-Zn. The images obtained show significant differences in the particle size, shape, and surface morphology for the monomers and dimers (Figures 4 and S21 Supplementary Material). Thus, monomer 1, which has no bulk substituents in *meso*-positions, forms particles with a high degree of crystallinity and distinct facets, whereas porphyrin 2 with the long-chain alkyl substituents has a friable flake structure. Dimer 4-Zn is characterized by a globular particle shape with

a particle size of about 100 nm. Dimer 5-Zn has a continuous porous surface with the inclusions of nanoparticles 70–100 nm in diameter.

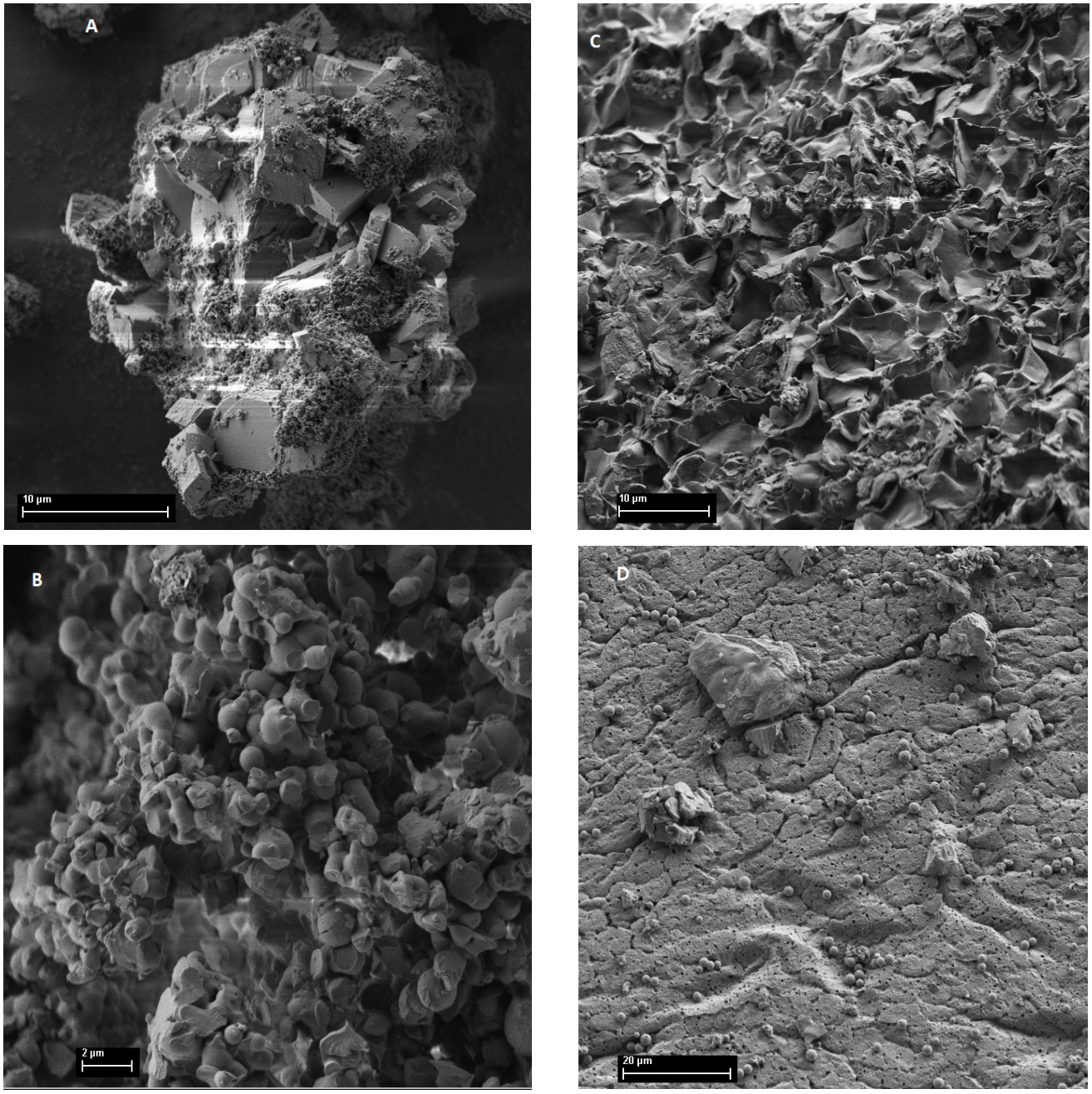

Figure 4. SEM images (**A**) porphyrin 1; (**B**) dimer 4-Zn; (**C**) porphyrin 2; (**D**) dimer 5-Zn.

2.5. Cytotoxicity

Preliminary measurements of cytotoxicity induced by monomeric porphyrins and their corresponding dimers were performed in the absence of light. The IC50 data for the HEK 293T cell line (human embryonic kidney) are presented in Table 4. As shown in Table 4, the IC50 value of the compounds tested for HEK293T cells was 111–720 µg/mL. Monomeric porphyrins 1, 1-Zn, 2-Zn have less toxic effect during 24 h incubation compared with the corresponding dimers. The received IC50 values are consistent with the results previously obtained for such class of compounds [43–45]. Also, introduction of Zn(II) into the macrocycles increased the toxicity of both monomers and dimers. The presence of long-chain alkyl substituents increased the solubility in the organic media but promotes increased

toxicity due to their higher hydrophobicity. As a result, for a successful application of such compounds, delivery vehicles are needed.

Table 4. Dark toxicity of the synthesized compounds on the HEK 293T cell line.

Compound	Toxicity IC50 (μg/mL)
	HEK293T
1	720.20 ± 35.51
1-Zn	575.10 ± 42.70
2-Zn	171.82 ± 28.63
4	147.71 ± 41.16
4-Zn	129.38 ± 36.44
5-Zn	111.84 ± 38.91

3. Experimental

Commercially available reagents were used without pretreatment. DMF was distilled over calcium oxide, and pyrrole was distilled over calcium hydride. For thin layer chromatography, TLC Silicagel 60 F254 plates (Merck, Darmstadt, Germany) were used to confirm the individuality of the compounds. Silica 60 silica gel 0.04–0.064 mm/230–400 mesh ASTM (Macherey-Nagel Gmb Hand Co. KG, Düren, Germany) was used for column chromatography. Porphyrins 1–3 were previously described [38,40]. NMR spectra were recorded in $CDCl_3$ on a BrukerMSL-300 pulsed Fourier spectrometer (Karlsruhe, Germany) with an operating frequency of 300 MHz; all measurements were performed on the δ scale, with an external standard tetramethylsilane. Mass spectra were recorded using a matrix-activated laser desorption/ionization time-of-flight mass spectrometer (MALDI-TOF) (Bruker Daltonics Inc., Bremen, Germany). SEM imaging was performed using a TESCAN AMBER GMH Electron Microscope (Brno, Czech Republic). Accelerating voltage was set at 1 keV with 5 mm working distance. Imaging was conducted using an ultra-high resolution mode with an Everhart-Thornley detector.

3.1. Solubilization in Surfactant Micelles

Micellar solutions of synthetic surfactants: cationic hexadecyltrimethylammonium bromide (CTAB, BioChemica&AppliChem, Gatersleben, Germany), anionic sodium *n*-dodecyl sulfate (SDS, Scharlau, Barcelona, Spain), and nonionic Triton X-100 (TX-100, Merck, Germany) were used for solubilization studies. Concentrations of surfactants five times the value of their critical micelle concentration (CMC) in water were used, taking into account the possible increase in CMC in the presence of traces of the organic solvent (~1% DMF). To perform spectral measurements, an aliquot of the stock porphyrin solution in DMF was added to the surfactant micellar solution upon stirring, and absorption and emission spectra were recorded 15–30 min after mixing.

3.2. Photochemical Measurements

Singlet oxygen quantum yields were evaluated by the chemical trapping method based on the dynamics of the absorbance decrease in the selective $^1O_2$ acceptor—1,3-diphenylisobenzofuran (DPBF, Acros Organics, Thermo Fisher Scientific, Waltham, MA, USA) at 415 nm (Figure S22 Supplementary Material), which was added to a porphyrin solution in DMF in the dark immediately before irradiation ($C_{DPBF} \approx 0.1$ mM). Unsubstituted tetraphenylporphyrin (TPP, $\Phi_\Delta = 0.52$) and its zinc complex (ZnTPP, $\Phi_\Delta = 0.74$) were used as standards [29,30]. The samples were irradiated in quartz cells at room temperature in air-saturated solutions in DMF using an optical system consisting of a 150 W halogen lamp, a three-lens spherical condenser with a reflector, thermal and UV filters, and a cut-off filter with $\lambda \geq 500$ nm. The light flux power was 10 mW/cm^2.

3.3. UV-Vis Spectroscopy

Electronic absorption spectra were recorded on a HACH DR-4000V spectrophotometer (Hach-Lange, Ames, IA, USA) in the wavelength range of 320–800 nm with 1 nm step in 10 mm quartz cells at room temperature. Steady-state fluorescence spectra were recorded using a Perkin Elmer LS-50 luminescence spectrometer (Perkin Elmer, Waltham, MA, USA) under similar conditions at the excitation wavelength corresponding to the absorption maximum of the porphyrin Sore band. Fluorescence quantum yields were calculated by a comparative method using TPP (Φ_F = 0.16) and ZnTPP (Φ_F = 0.033) as standards [42].

3.4. MTT Test

The cancer cell line HEK293T was purchased from the cell bank of N. N. Blokhin National Medical Research Center of Oncology of the Russian Ministry of Health. Cytotoxicity of the compounds obtained was determined using the MTT test on the human embryonic renal cell line HEK293T. The essence of the method is the metabolic conversion of MTT to diformazan by NADPH*H-dependent cell oxidases whose activity increases during mitogenesis. The day before the experiment, cells were plated in a 96-well plate at 2×10^5 cells per well in a complete DMEM nutrient medium and incubated for 24 h at 37 °C in a CO_2 incubator until 75% confluence. The difference in the absorbance of the solution at 570 and 650 nm was determined on a Thermo Scientific spectrophotometer (Multiskan FC, Waltham, MA, USA). The number of the living cells was calculated as the ratio of the absorbance in the well with a given concentration to that of the control. Each value was obtained by averaging at least three parallel measurements.

3.5. Synthesis

General methodology for the preparation of dimeric porphyrins based on α,α′-dibromo-o-xylene:

A solution of 1 eq. of hydroxyl-containing porphyrin or its Zn(II) complex and 5 eq. of Cs_2CO_3 in 5 mL of DMF was boiled for 30 min, then 0.5 eq. of 1,2-bis(bromomethyl)benzene was added. The reaction mixture was boiled for 5 h. The course of the reaction was monitored by TLC. DMF was removed under vacuum, and the resulting mixture was purified by column chromatography on silica gel in the system CH_2Cl_2:C_6H_{14} = 4:1.

3.5.1. Compound 4

Compound 4 was obtained from 0.050 g (0.072 mmol) of porphyrin 1, 0.017 g (0.360 mmol) of cesium carbonate, and 0.0095 g (0.036 mmol) of α,α-dibromo-*ortho*-xylene. Yield: 0.048 g (89%), purple powder, Rf 0.85 (CH_2Cl_2). UV-vis, λ, nm (lgε): 418.1 (5.78); 517.0 (4.51); 552.9 (4.14); 595.0 (3.93); 649.9 (3.79). ^{1}H NMR ($CDCl_3$, δ, ppm): 8.82 (8H, m, βPyr), 8.74 (4H, m, βPyr), 8.55 (4H, βPyr), 8.30 (2H, m, 2,6Ar-H), 8.22 (4H, m, 2,6Ar-H), 8.18 (4H, m, 2,6Ar-H), 7.93 (6H, m, 2,6Ar-H), 7.93 (4H, m, 3,5Ar-H), 7.84 (8H, m, 3,5Ar-H), 7.77 (6H, m, 4Ar-H), 7.55 (4H, m, αα′ββ′xylene), 7.40 (4H, s, 3,5Ar-H), 5.94 (4H, s, -OCH2), −2.78 (4H, s, NH Pyr). ^{13}C NMR ($CDCl_3$, δ, ppm): 141.86, 141.67, 139.62, 138.54, 135.47, 135.33, 135.05, 134.76, 134.21, 134.01, 129.04, 128.47, 126.13, 125.91, 119.81, 119.63, 119.61, 119.52, 112.66, 68.18. MALDI-TOF-MS, *m*/*z*: found 1364.586 $[M]^+$, calculated for $C_{96}H_{66}N_8O_2$: 1363.604.

3.5.2. Compound 5

Compound 5 was prepared from 0.036 g (0.03 mmol) of porphyrin 2, 0.049 g (0.15 mmol) of cesium carbonate, and 6.3 mg (0.024 mmol) of α,α-dibromo-*ortho*-xylene. Yield: 0.029 g (79%). UV-vis (CH_2Cl_2, λmax/nm (lgε)): 422.1 (5.92); 518.8 (4.49); 554.6 (4.26); 589.0 (4.06); 649.6 (3.96). ^{1}H NMR ($CDCl_3$, δ, ppm): ^{1}H NMR ($CDCl_3$, δ, ppm): 9.03 (12H, m, βPyr), 8.79 (4H, m, βPyr), 8.36 (2H, m, 2,6Ar-H), 8.24 (8H, m, 2,6Ar-H), 8.06 (6H, s, 2,6Ar-H), 7.77(8H, m, 3,5Ar-H), 7.60 (6H, m,), 7.55 (4H, m, xylene), 7.42 (2H, m, 3,5Ar-H), 5.55 (4H, s, -OCH_2 xylene), 4.24 (12H, m, OCH_2), 2.10–2.00 (12H, m, OCH_2CH_2), 1.74–1.59 (12H, $O(CH_2)_2CH_2$), 1.55–1.27 (96H, br m, $O(CH_2)_3(CH_2)_8$), 0.91 (18H, m, CH_3). ^{13}C NMR ($CDCl_3$, δ, ppm): 158.60, 150.76, 150.06, 142.96, 135.40, 134.54, 131.95, 131.16, 129.42, 128.81, 127.57, 126.64,

121.26, 113.12, 112.43, 112.08, 68.82, 68.34, 67.81, 39.01, 31.89, 30.00, 29.36, 26.59, 26.59, 23.71, 22.99, 22.53, 14.34, 11.28, 11.28, 0.74. MALDI-TOF-MS *m*/*z*: found 2470.406 $[M+1]^+$; calculated for $C_{168}H_{210}N_8O_8$ 2468.53.

3.5.3. Compound 4-Zn

Compound 4-Zn was prepared from 0.050 g (0.072 mmol) of porphyrin 1-Zn, 0.117 g (0.36 mmol) of cesium carbonate, and 9.5 mg (0.036 mmol) of α,α-dibromo-ortho-xylene. Yield: 0.051 g (90%), purple powder, R_f 0.80 (CH_2Cl_2). UV-vis (CH_2Cl_2, λmax/nm (lgε)) 426 (5.78), 555 (4.61), 595.5 (3.96). ^{1}H NMR ($CDCl_3$, δ, ppm): 8.88 (4H, d, *J* = 4.95 Hz, βPyr), 8.83 (4H, d, *J* = 4.95 Hz, βPyr), 8.79 (4H, d, *J* = 4.77 Hz, βPyr), 8.71 (2H, d, *J* = 4.77 Hz, βPyr), 8.23 (4H, m, 2,6Ar-H), 8.17 (4H, d, *J* = 8.5 Hz, 2,6Ar-H), 8.05 (8H, d, *J* = 8 Hz, 2,6Ar-H), 7.76 (6H, m, 4Ar-H), 7.63 (2H, m, αα′ xylene), 7.60 (2H, m, ββ′ xylene), 7.57 (4H, s, 3,5Ar-H), 7.54 (6H, m, 3,5Ar-H), 5.58 (4H, s, -OCH_2). ^{13}C NMR ($CDCl_3$, δ, ppm): 158.78, 142.61, 136.26, 135.64, 135.24, 134.80, 134.53, 131.40, 129.62, 129.47, 128.62, 127.93, 127.77, 126.92, 126.74, 120.53, 113.49, 68.80. MALDI-TOF-MS, *m*/*z*: found 1487.093 $[M+1]^+$; calculated for $C_{96}H_{64}N_8O_2Zn_2$: 1486.360.

3.5.4. Compound 5-Zn

Compound 5-Zn was prepared from 0.050 g (0.072 mmol) of porphyrin 2-Zn, 0.117 g (0.36 mmol) of cesium carbonate, and 9.5 mg (0.036 mmol) of α,α-dibromo-ortho-xylene. Yield: 0.051 g (90%), purple powder, R_f 0.85 (CH_2Cl_2). UV-vis (CH_2Cl_2, λmax/nm (lgε)): 429.5 (5.98); 556.0 (4.77); 596.7 (4.14). ^{1}H NMR ($CDCl_3$, δ, ppm): ^{1}H NMR ($CDCl_3$, δ, ppm): 8.94–8.83 (12H, m, βPyr), 8.74 (2H, d, *J* = 4.77 Hz, βPyr), 8.63 (2H, d, *J* = 4.58 Hz, βPyr), 8.27 (4H, m, 2,6Ar-H), 8.18–8.11 (8H, m, 2,6Ar-H), 8.06 (4H, d, *J* = 8.62 Hz, 2,6Ar-H), 7.76–7.72 (1H, m, α xylene), 7.68 (2H, m, ββ′ xylene), 7.57 (1H, m, α′ xylene), 7.31–7.25 (10H, m, 3,5Ar-H), 7.26–7.22 (6H, m, 3,5Ar-H), 6.36 (4H, s, -OCH_2 xylene), 4.27–4.15 (12H, m, OCH_2), 2.07–1.90 (12H, m, OCH_2CH_2), 1.79–1.59 (12H, $O(CH_2)_2CH_2$), 1.53–1.27 (96H, br m, $O(CH_2)_3(CH_2)_8$), 0.92 (18H, m, CH_3). ^{13}C NMR ($CDCl_3$, δ, ppm):158.79, 158.34, 136.94, 135.59, 134.97, 134.74, 133.93, 131.03, 130.12, 128.99, 128.12, 127.20, 119.91, 119.70, 119.44, 115.17, 113.19, 111.93, 68.70, 67.64, 31.92, 29.10, 26.22, 22.53, 14.20, 1.30. MALDI-TOF-MS *m*/*z*: found 2632.989 $[M+K]^+$; calculated for $C_{168}H_{208}N_8O_8Zn_2K$ 2633.420.

3.5.5. Compound 6

Compound 6 was prepared from 0.050 g (0.072 mmol) porphyrin 3, 0.019 g (0.072 mmol) α,α-dibromo-ortho-xylene, and 0.014 g (0.360 mmol) of cesium carbonate. Yield: 0.049 g (85%), purple powder, R_f 0.75 (CH_2Cl_2). UV-vis (CH_2Cl_2, λmax/nm (lgε)): 423.0 (5.39), 551.5 (4.21), 591.0 (3.86). ^{1}H NMR ($CDCl_3$, δ, ppm): 8.98 (2H, d, *J* = 4.23 Hz, βPyr), 8.83 (6H, m, βPyr), 8.21 (6H, m, 2,6Ar-H), 8.17 (2H, d, *J* = 8.39 Hz, 2,6Ar-H), 8.19 (4H, m, 2,6Ar-H); 7.77–7.79 (6H, m, 4Ar-H); 7.40–7.45 (2H, m, ββ′CH); 7.32–7.39 (6H, m, 3,5ArH), 7.29–7.32 (2H, m, 3,5Ar-H), 7.07 (2H, d, *J* = 9.31 Hz, α,α′ CH), 4.98 (4H, br s, $N(CH_2)_2$). MALDI-TOF-MS *m*/*z*: found $[M]^+$ 795.120; calculated for $C_{54}H_{35}N_5Zn$: 795.250.

4. Conclusions

In conclusion, new dimers of porphyrins and their zinc complexes were prepared with good yields and characterized by a number of methods. The nucleophilic substitution of bromine in α,α′-dibromo-o-xylene by hydroxy-substituted porphyrins leads to the formation of covalently linked dimers. A similar reaction with amino porphyrins leads to a heterocyclization reaction and the formation of an isoindoline derivative. The highest yield in this reaction was achieved using an excess of cesium carbonate. An investigation of photophysical properties shows the influence of peripheric long-chain alkoxy-substituents and a central metal atom. Thus, alkoxy-substituted compounds possess higher fluorescence quantum yields in comparison with the unsubstituted compounds. All zinc complexes are characterized by higher singlet oxygen quantum yields and lower fluorescence intensity compared to the metal-free porphyrins. Spectral-luminescent properties in model micellar

systems show effective stabilization of a monomolecular form of synthesized compounds, using nonionic surfactant Triton X-100. Ionic surfactants (SDS, CTAB) provide only partial solubilization for the received compounds. Cytotoxicity of received dimers significantly increased compared to corresponding monomers. However, these compounds surely need a delivery vehicle, such as liposomes. Our studies suggest that dimeric porphyrins have good potential for photodynamic therapy and give the further direction of dimer modification.

Supplementary Materials: The following supporting information can be downloaded at: https://www.mdpi.com/article/10.3390/inorganics11100415/s1.

Author Contributions: Manuscript conception, K.A.Z.; writing—review and editing, A.S.N.; writing and original draft preparation K.A.Z. and M.A.G.; synthesis of derivatives A.A.Z.; solubilization and physicochemical properties study M.A.G. and O.V.G.; editing, data analysis, and interpretation, A.V.L., M.A.G. and N.A.B. All authors have read and agreed to the published version of the manuscript.

Funding: The reported study was funded by the Russian Science Foundation, project number 22-73-10176.

Data Availability Statement: The data presented in this study are available in this article and Supplementary Materials.

Acknowledgments: A.S.N. is grateful to the RUDN University Strategic Academic Leadership Program. This work was performed using the equipment of the Shared Science and Training Center for Collective Use of RTU MIREA and supported by the Ministry of Science and Higher Education of the Russian Federation.

Conflicts of Interest: The authors declare no conflict of interest.

References

1. Ethirajan, M.; Chen, Y. The role of porphyrin chemistry in tumor imaging and photodynamic therapy. *Chem. Soc. Rev.* **2011**, *40*, 340–362. [CrossRef] [PubMed]
2. Jenni, S.; Sour, A. Molecular Theranostic Agents for Photodynamic Therapy (PDT) and Magnetic Resonance Imaging (MRI). *Inorganics* **2019**, *7*, 10. [CrossRef]
3. Yang, F.; Xu, M. Spotlight on porphyrins: Classifications, mechanisms and medical applications. *Biomed. Pharmacother.* **2023**, *164*, 114933. [CrossRef] [PubMed]
4. Ding, Y.; Wang, J. Development of porphyrin-based fluorescent sensors and sensor arrays for saccharide recognition. *Chin. Chem. Lett.* 2023; 109008, *in press*. [CrossRef]
5. Balu, K.; Kaliyamoorthy, S. Porphyrins and ZnO hybrid semiconductor materials: A review. *Inorg. Chem. Commun.* **2023**, *154*, 110973. [CrossRef]
6. Plekhova, N.; Shevchenko, O. Development of Novel Tetrapyrrole Structure Photosensitizers for Cancer Photodynamic Therapy. *Bioengineering* **2022**, *9*, 82. [CrossRef]
7. Tian, J.; Huang, B. Recent advances of multi-dimensional porphyrin-based functional materials in photodynamic therapy. *Coord. Chem. Rev.* **2020**, *420*, 213410. [CrossRef]
8. Park, J.M.; Lee, J.H. Applications of porphyrins in emerging energy conversion technologies. *Coord. Chem. Rev.* **2020**, *407*, 213157. [CrossRef]
9. Li, C.; Wang, Y. Direct [4 + 2] Cycloaddition to Isoquinoline-Fused Porphyrins for Near-Infrared Photodynamic Anticancer Agents. *Org. Lett.* **2022**, *24*, 175–180. [CrossRef]
10. Smirnov, A.S.; Grin, M.A. Synthesis and properties of Cu- and Pd-complexes of cyclen conjugates with pheophorbide and bacteriopheophorbide. *Fine Chem. Technol.* **2019**, *14*, 95–103. [CrossRef]
11. Mironov, A.F.; Ostroverkhov, P.V. Amino acid derivatives of natural chlorins as a platform for the creation of targeted photosensitizers in oncology. *Fine Chem. Technol.* **2020**, *15*, 16–33. [CrossRef]
12. Antipin, I.S.; Alfimov, M.V. Functional supramolecular systems: Design and applications. *Russ. Chem. Rev.* **2021**, *90*, 895. [CrossRef]
13. Burrell, A.K.; Officer, D.L. Synthetic routes to multiporphyrin arrays. *Chem. Rev.* **2001**, *101*, 2751–2796. [CrossRef] [PubMed]
14. Satake, A.; Kobuke, Y. Artificial photosynthetic systems: Assemblies of slipped cofacial porphyrins and phthalocyanines showing strong electronic coupling. *Org. Biomol. Chem.* **2007**, *5*, 1679–1691. [CrossRef] [PubMed]
15. Mchiri, C.; Gassoumi, B. New cadmium(II) porphyrin-based coordination dimer: Experimental and theoretic studies. *J. Solid State Chem.* **2022**, *314*, 123364. [CrossRef]

16. Tyurin, V.S.; Yashchuk, Y.P. Supramolecular self-assembly of 5,10,15,20-tetrakis-(3-hydroxyphenyl)porphyrinatozinc with some transition metals and bidentate ligands. *Russ. J. Org. Chem.* **2008**, *44*, 1378–1383. [CrossRef]
17. Martin, K.E.; Wang, Z. Donor−Acceptor Biomorphs from the Ionic Self-Assembly of Porphyrins. *J. Am. Chem. Soc.* **2010**, *132*, 8194–8201. [CrossRef]
18. Mamardashvili, G.M.; Kaigorodova, E.Y.; Lebedev, I.S.; Khodov, I.A.; Mamardashvili, N.Z. Supramolecular assembly of hydrophilic Co(III)-porphyrin with bidentate ligands in aqueous buffer media. *Inorg. Chim. Acta* **2022**, *538*, 120972. [CrossRef]
19. Ravikumar, M.; Farley, C. 1,3–diyne bridged porphyrin dimers via Cu-catalysis: Synthesis, optical properties and application in fullerene binding. *J. Mol. Struct.* **2021**, *1240*, 130570. [CrossRef]
20. Moreira, L.; Valbo, J. Conjugated Porphyrin Dimers: Cooperative Effects and Electronic Communication in Supramolecular Ensembles with C60. *J. Am. Chem. Soc.* **2016**, *138*, 15359–15367. [CrossRef]
21. Luechai, A.; Pootrakulchote, N. Photosensitizing triarylamine- and triazine-cored porphyrin dimers for dye-sensitized solar cells. *Organomet. Chem.* **2014**, *753*, 27–33. [CrossRef]
22. Piradi, V.; Xu, X. Panchromatic Ternary Organic Solar Cells with Porphyrin Dimers and Absorption-Complementary Benzodithiophene-based Small Molecules. *ACS Appl. Mater. Interfaces* **2019**, *11*, 6283–6291. [CrossRef] [PubMed]
23. Okuda, Y.; Fukui, N. A meso–meso β-β β-β Triply Linked Subporphyrin Dimer. *Angew. Chem. Int. Ed.* **2017**, *56*, 12317. [CrossRef] [PubMed]
24. Bhuse, D.V.; Bhuse, V.M. Ant-like small molecule metal-free dimeric porphyrin sensitizer for true energy-generating DSSC with 9.3% efficiency. *J. Mater. Sci. Mater. Electron.* **2022**, *33*, 14305–14322. [CrossRef]
25. Xia, Y.; Shuai, L. Designing bifuncitonal molecular devices with a metalloporphyrin dimer. *Phys. Chem. Chem. Phys.* **2020**, *22*, 4080–4085. [CrossRef] [PubMed]
26. Garcia, G.; Hammerer, F. Carbohydrate-conjugated porphyrin dimers: Synthesis and photobiological evaluation for a potential application in one-photon and two-photon photodynamic therapy. *Bioorg. Med. Chem.* **2013**, *21*, 153–165. [CrossRef]
27. Mazur, L.M.; Roland, T. Efficient Singlet Oxygen Photogeneration by Zinc Porphyrin Dimers upon One- and Two-Photon Excitation. *J. Phys. Chem. B* **2019**, *123*, 4271–4277. [CrossRef]
28. Schmitt, J.; Jenni, S. A Porphyrin Dimer–GdDOTA Conjugate as a Theranostic Agent for One- and Two-Photon Photodynamic Therapy and MRI. *Bioconj. Chem.* **2018**, *29*, 3726–3738. [CrossRef]
29. Mohamed, E.A.; Zahran, Z.N. Covalent bonds immobilization of cofacial Mn porphyrin dimers on an ITO electrode for efficient water oxidation in aqueous solutions. *J. Catal.* **2017**, *352*, 293–299. [CrossRef]
30. Kumar, R.S.; Ryu, J. Synthesis, characterization, and photocatalytic disinfection studies of porphyrin dimer/TiO2-based photocatalyst. *J. Mol. Struct.* **2021**, *1236*, 130276. [CrossRef]
31. Yaschuk, Y.P.; Tyurin, V.S. Trimer Porphyrin Star. *Macroheterocycles* **2012**, *5*, 302–307. [CrossRef]
32. Higashino, T.; Kurumisawa, Y. ABC–ABC-Type Directly meso–meso Linked Porphyrin Dimers. *Chem. Eur. J.* **2019**, *25*, 538–547. [CrossRef]
33. Belcher, W.J.; Burrell, A.K. The synthesis of specifically metallated heterobimetallic dimeric porphyrins. *J. Porphyr. Phthalocyanines* **2002**, *6*, 720–736. [CrossRef]
34. Fletcher, J.T.; Therien, M.J. Transition-Metal-Mediated [2 + 2 + 2] Cycloaddition Reactions with Ethyne-Containing Porphyrin Templates: New Routes to Cofacial Porphyrin Structures and Facially-Functionalized (Porphinato)metal Species. *J. Am. Chem. Soc.* **2000**, *122*, 12393–12394. [CrossRef]
35. Takai, A.; Gros, C. Enhanced Electron-Transfer Properties of Cofacial Porphyrin Dimers through π–π Interactions S. *Chem. Eur. J.* **2009**, *15*, 3110–3122. [CrossRef] [PubMed]
36. Pushkarev, V.E.; Tolbin, A.Y. Sandwich Double-Decker Lanthanide(III) "Intracavity" Complexes Based on Clamshell-Type Phthalocyanine Ligands: Synthesis, Spectral, Electrochemical, and Spectroelectrochemical Investigations. *Chem. Eur. J.* **2012**, *18*, 9046–9055. [CrossRef]
37. Tolbin, A.Y.; Pushkarev, V.E. Directed synthesis of bi- and polynuclear clamshell-type phthalocyanines and their physico-chemical investigations. *J. Porphyr. Phthalocyanines* **2012**, *16*, 341–350. [CrossRef]
38. Zhdanova, K.A.; Zhdanov, A.P. Synthesis of amino-containing meso-aryl-substituted porphyrins and their conjugates with the closo-decaborate anion. *Russ. Chem. Bull.* **2014**, *1*, 194–200. [CrossRef]
39. Adler, A.D.; Longo, E.R. Mechanistic Investigations of Porphyrin Syntheses. I. Preliminary Studies on ms-Tetraphenylporphin. *J. Am. Chem. Soc.* **1964**, *86*, 3145–3149. [CrossRef]
40. Gradova, M.A.; Gradov, O.V. Self-assembly of amphiphilic meso-aryl-substituted porphyrin derivatives in the presence of surfactants. *J. Porphyr. Phthalocyanines* **2020**, *24*, 505–514. [CrossRef]
41. Taniguchi, M.; Lindsey, J.S. Comprehensive review of photophysical parameters (ε, Φf, τs) of tetraphenylporphyrin (H2TPP) and zinc tetraphenylporphyrin (ZnTPP)—Critical benchmark molecules in photochemistry and photosynthesis. *J. Photochem. Photobiol. C Photochem. Rev.* **2021**, *46*, 100401. [CrossRef]
42. Ormond, A.B.; Freeman, H.S. Effects of substituents on the photophysical properties of symmetrical porphyrins. *Dye. Pigments* **2013**, *96*, 440–448. [CrossRef]
43. Spiller, W.; Kliesch, H. Singlet Oxygen Quantum Yields of Different Photosensitizers in Polar Solvents and Micellar Solutions. *J. Porphyr. Phthalocyanines* **1998**, *2*, 145–158. [CrossRef]

44. Yao, G.; Zhang, Z. Synthesis of three novel imidazolyl-appended porphyrins and their cytostatic and phototoxic activity on A431 cells. *J. Porphyr. Phthalocyanines* **2013**, *17*, 1113–1119. [CrossRef]
45. Zhdanova, K.A.; Ivantsova, A.V. Design of A3B-Porphyrin Conjugates with Terpyridine as Potential Theranostic Agents: Synthesis, Complexation with Fe(III), Gd(III), and Photodynamic Activity. *Pharmaceutics* **2023**, *15*, 269. [CrossRef]

Disclaimer/Publisher's Note: The statements, opinions and data contained in all publications are solely those of the individual author(s) and contributor(s) and not of MDPI and/or the editor(s). MDPI and/or the editor(s) disclaim responsibility for any injury to people or property resulting from any ideas, methods, instructions or products referred to in the content.